We are IntechOpen, the world's leading publisher of Open Access books Built by scientists, for scientists

4,800
Open access books available

122,000
International authors and editors

135M
Downloads

Our authors are among the

154
Countries delivered to

TOP 1%
most cited scientists

12.2%
Contributors from top 500 universities

CLARIVATE ANALYTICS BOOK CITATION INDEX INDEXED

WEB OF SCIENCE™

Selection of our books indexed in the Book Citation Index in Web of Science™ Core Collection (BKCI)

Interested in publishing with us?
Contact book.department@intechopen.com

Numbers displayed above are based on latest data collected.
For more information visit www.intechopen.com

16

Frequency Domain Skin Artifact Removal Method for Ultra-Wideband Breast Cancer Detection

Arash Maskooki, Cheong Boon Soh, Erry Gunawan and Kay Soon Low
Nanyang Technological University
Singapore

1. Introduction

According to the Center for Disease Control and Prevention (CDC) (Center for Disease Control and Prevention (CDC), 2007) and American Cancer Society (ACS) (American Cancer Society (ACS), 2007), breast cancer is the most prevalent type of cancer among women only after skin cancer and the number two cause of cancer death in women. Among every 8 women in U.S. one has breast cancer. In addition, about 2.5 million survivors of breast cancer are living in the United States and it is estimated that 40,170 lives perished due to this mortal disease in 2009. Many risk factors have been associated with breast cancer including, but not limited to, gender, age, family history, race and lifestyle (American Cancer Society (ACS), 2007). Some of these risk factors could not be controlled such as age or family history. In contrast, factors such as life style could be changed to prevent or reduce the chance of breast cancer. Various techniques are practiced today for treating breast cancer. Nevertheless, in all treatment methods early detection is a crucial factor. Detecting breast cancer in early stages can lead to more efficient treatment and comfort for the patient. Hence, an accurate diagnosis modality for breast cancer detection can save many lives annually.

Currently, X-Ray mammography is the gold standard method in detecting breast cancer and is used widely due to relatively easy access to the equipment. In this method, a low dose of X-Ray is used to obtain a mapping of the distribution of the tissue density inside the compressed breast. Mammography can be used for both screening and diagnosis of breast cancer. In screening mammography, X-Ray imaging of the breast is used in women with no signs of the breast cancer for the purpose of investigation of the breast tissue changes and examining the lesions inside the breast. As a diagnostic tool, X-Ray mammography could be used to assess the malignancy of the lesions that has already been found in the breast. It has been shown that mammography can reduce the mortality rate due to breast cancer (J. Elwood and B. Cox and A. Richardson, 1993) because detecting breast cancer in the early stages can lead to a more efficient treatment. Although X-Ray mammography has benefits such as ease of use, availability and being reasonably accurate, it is not a perfect method for screening and diagnosing breast cancer. A major drawback of X-Ray mammography is the danger of exposing the patient to a low dose of ionizing radiation which can increase the risk of cancer. This makes X-ray mammography a less suitable tool for screening and more suitable for diagnosis. In addition, to avoid a blurred image and preserve the uniformity of the tissue, the breast is compressed before X-Ray imaging which can be uncomfortable for the patients (Fear et al., 2002).

Another modality based on Ultra-Wide Band (UWB) pulse confocal imaging radar for screening and possibly diagnosis of breast cancer has been suggested and investigated in recent years (Li & Hagness, 2001). UWB imaging of the breast employs malignant tissue's significant dielectric contrast to detect the location of the tumor relative to an antenna array. To obtain a 2-D or 3-D (depending on the application) map of dielectric contrast inside the breast medium, an array of antenna around the breast transmit a UWB pulse sequentially and record the backscattered signal. In the next step, the backscattered signals are synthetically focused at a synthetic focal point. To focus the beam at the synthetic focal point, the travel time between the antenna and the synthetic focal point is calculated and the energy received from that point in all channels in the antenna array are added together. Existence of a strong scattering point (high contrast in dielectric value) at the synthetic focal point results in a coherent summation of pulse energy and hence a high total energy value assigned to that point. On the other hand, if no scattering point is present at the synthetic focal point, energy values will add incoherently and the total energy value assigned to that location won't be so high. To produce a 2D or 3D image of the breast region, the synthetic focal point is scanned through all the breast region and the summation of the acquired energy values are mapped as the pixel value at that location.

In contrast to the X-ray mammography, UWB confocal imaging does not expose the patient to any ionizing radiation. This means that it can be used frequently as an screening tool specially for younger women. In addition, the uncomfortable breast compression is eliminated is this modality.

Although it has been shown that the cancerous tumors can be located by UWB breast imaging, there are still issues that must be addressed. One of these issues is the problem of the surface skin backscatter. Human breast skin has a high dielectric contrast with both air and skin tissue. This will produce a strong backscatter from the skin surface in the received signal. Although skin backscatter has its major components in the early time of the received signal, it continues to affect parts of the late time response. The problem is that the late time effects of the skin backscatter are still strong enough to mask the weak tumor reflection completely. Hence, the skin effects should be removed from the response prior to the imaging process. A simple method to remove the skin artifact is to mask out the early time part of the signal. However, as mentioned before, skin artifact continues its effect to the late time response and masking out the early time part of the signal would not remove the late time effects. Another problem of the simple masking method is that prior to the imaging process the location of the tumor is not known. Hence, masking the early time part of the signal might remove the tumor reflection. A more practical method has been suggested by researchers based on averaging. In averaging method, the backscattered signal is averaged over all signals from different antennas in the array. The average is then subtracted from the individual signals. The idea is that the skin reflection would appear in the average because it is similar in all channels and will add coherently, but the tumor response has different locations in different channels and would not add up coherently and hence would not appear in the average. Although averaging can significantly suppress the early time portion of the skin reflection, it is not able to remove the late time parts of the artifact. In addition, averaging removes parts of the reflection from the tumor especially in cases where the tumor is equidistant from different antennas. As an improvement over averaging, an averaging based filtering process is proposed in literature to remove the skin artifact. Although filtering greatly improves the skin backscatter removal, it still deteriorates the tumor response. Furthermore, the same as averaging method, it will

remove the tumor reflection together with the skin artifact when the tumor is equidistant to several antennas in the array.
This chapter introduces a frequency domain approach to the skin artifact removal problem in UWB breast cancer detection. In this approach, the received signal is first converted into the frequency domain. Then, the skin related information is identified and removed from the frequency domain response. The signal is then converted back to the time domain and used for the imaging process. This approach does not affect the tumor response as it processes each signal individually and does not incorporate any subtraction or addition to the signals. Besides, the skin reflection is eliminated from both early time and late time responses. In addition, it is shown that the frequency domain approach can preserve the tumor response when the tumor is located equidistant to all antennas in the array, such as central axis of the array. Using computer simulations, the frequency domain approach is compared with the existing averaging based methods in different scenarios and is shown to be able to outperform the current existing methods.
This chapter is organized as follows. The next section provides a brief overview of the confocal imaging method in UWB breast cancer detection. In Section 3, the skin artifact problem and existing methods to overcome this problem are described. Section 4 introduces the frequency domain approach to remove the skin artifact. In Section 5, performance of the frequency domain approach is compared with the existing methods through computer simulations in different cases and each case is discussed in detail. Finally, Section 6 will conclude this chapter.

2. Confocal Microwave Imaging (CMI) in UWB breast imaging

To obtain the tumor signature, breast is illuminated by a UWB microwave pulse from a number of antennas arranged in a planar configuration over the breast or in a circular configuration around the breast (Fear et al., 2002). Due to the contrast between dielectric properties of the tumor and the normal breast tissue, malignant tumors have a significant scattering cross section compared to the normal tissue and benign tumor types (Hagness et al., 1998). To obtain a high resolution in the imaging process, the pulse bandwidth has to be as high as possible. However, frequencies higher than 10 GHz will face a dramatic attenuation inside the human body and the breast medium. Hence, the upper limit for frequency content of the signal is about 10 GHz. This limit ensures enough penetration for human breast imaging (Fear & Stuchly, 2000).
To obtain enough penetration for the UWB imaging of the breast, the antenna is excited by a differentiated Gaussian pulse (Fear et al., 2002):

$$V(t) = (t - t_0)e^{-(\frac{t-t_0}{\tau})^2} \tag{1}$$

where $t_0 = 4\tau$ and $\tau = 0.0625ns$. The resulting signal has temporal duration (full-width half-maximum) of 0.17 ns and approximately 6 GHz bandwidth with maximum power near to 4GHz. Figure 1 shows the temporal pulse shape and its frequency spectrum (Fear et al., 2002).
The heterogeneous nature of the breast medium produces clutter in the UWB signature of the tumor which makes detecting the tumor difficult or in some cases impossible. To overcome this problem, a modified version of UWB Ground Penetrating Radar (GPR) is suggested for breast medium to amplify the tumor signature and eliminate the clutter (Hagness et al., 1998). In this method, clutter suppression is carried out by coherent addition of the tumor responses from all channels. To spatially focus the signal at the candidate location, the backscattered

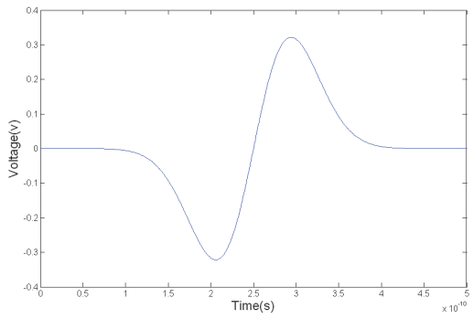

(a) Differentiated Gaussian Pulse

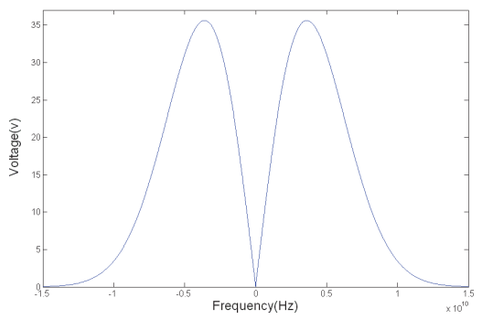

(b) Frequency Spectrum of Differentiated Gaussian Pulse

Fig. 1. Pulse Waveform

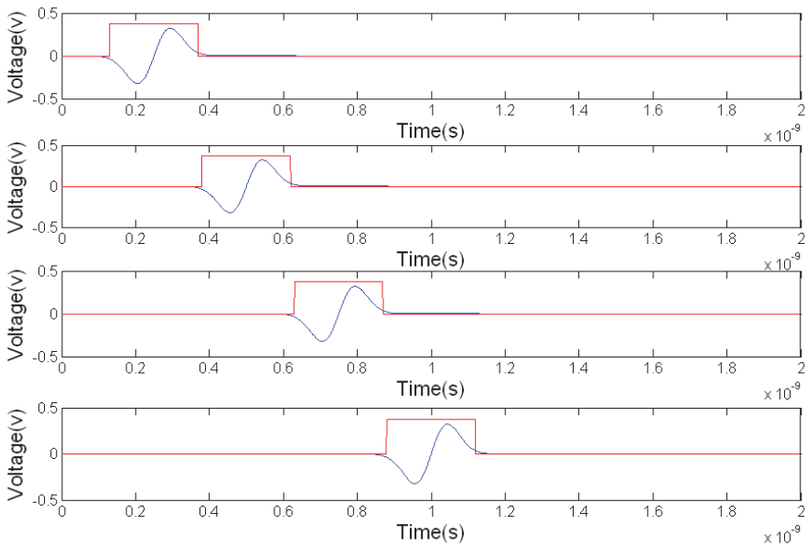

Fig. 2. A time window is applied on different channel responses in Confocal Imaging Process

signal is time shifted and summed based on the pulse travel time to the synthetic focal point. The energy value of the windowed portion of the signals from all the channels are calculated and summed up to form a pixel value for the image of the breast. The synthetic focal point is then scanned through the entire breast medium by appropriately changing the time shifts and windowing to achieve a 2D or 3D image of the breast. As mentioned before, existence of a strong scatterer at the synthetic focal point would produce a replica of the pulse at the corresponding time instance in the backscattered signal in all channels. Hence, summation of this portion of the response from all channels yields a high energy value which points to the existence of a scatterer. However, if only clutter and noise are the dominant components at the focal point, the energy levels do not add coherently and the clutter will be suppressed (Fear & Stuchly, 2000). Figure 2 depicts the windowing and summation process. The window length is chosen equal to the temporal duration of the original pulse to include the whole backscattered energy.

3. Skin backscatter removal

The signal received by the antenna contains contributions from lesions in the breast, clutter due to heterogeneity of the tissue and skin backscatter. The skin backscatter artifact is in the orders of magnitude larger than the other parts of the signal and can swamp the tumor response. Thus, to detect the tumor, skin response should be removed from the signal. This section describes and reviews the existing skin artifact removal algorithms.

3.1 Time window

The simplest way to get rid of the skin artifact is to mask out the early time part of the response. This method could be considered as multiplying a time window which is a step function of zero amplitude when the skin response exists and amplitude one in the rest of the time interval (Zhi & Chin, 2006). However, this method could not be used in practice. The problem is that there is no clear border between early time and late time parts of the backscattered signal. In addition, skin reflection can be present in the late time response and mask the tumor backscatter. Hence masking the early time part of the signal may remove the tumor response as well. This is because the location of the tumor reflection is not a priori information.

3.2 Averaging

A more practical method to remove the skin reflection from the backscattered signal is to use the average of all channels to reconstruct and remove the skin reflection (Li & Hagness, 2001). In this method, the average of the backscattered responses from several antenna elements is subtracted from the response of each element. The idea in averaging method is that the skin response is similar in different channels. This is because the skin structure is assumed symmetric in the view of all elements of the antenna array. To compensate for the variations in each element's distance from skin surface, all responses are aligned to the local maximum of the early time response (which corresponds to the skin backscatter). When the signals in different channels are averaged, the similar parts such as skin backscatter will add up coherently and hence appear in the averaged signal. However, other reflections such as tumor and clutter backscatters differ in amplitude and location from channel to channel. The tumor reflection is at different time instants in different channels. This is because of the difference in the relative distance of the tumor to each antenna element. Hence the tumor signature will add incoherently in the averaging process and is suppressed in the average signal. Thus, removing the average from the signal removes mostly the skin artifact.

Averaging best works when the skin reflection is similar in all channels. In such case, it can totally remove skin artifact from the data. Nevertheless, skin structure is not the same all over the breast and this affects the similarity of the skin reflections at different receivers. One of the factors that changes the skin response in different locations is the variation in skin thickness in different parts of the breast (Ulger et al., 2003). Another contributing factor is the heterogeneity of the breast tissue under the skin surface which can cause variations in the skin backscatter.

As mentioned above, skin response does vary from channel to channel and this variation affects the ability of the averaging in removing the skin artifact thoroughly. Another inherent problem of the averaging method is the distortion to the possible tumor reflection. This is because during the averaging process the tumor and clutter responses from all channels are added and averaged incoherently. This average is then subtracted from each channel and

consequently an unwanted averaged version of the clutter and tumor response is added to each channel which deteriorates the tumor signature and is undesirable.

3.3 Weighted average (Space-Time filter)

An improvement over averaging method is the Space-Time filter proposed in (Bond et al., 2003). In this method, a weighted average algorithm makes use of the similarity of the early time responses in antenna elements to estimate and remove the artifacts in this portion of the received signal. To do this, a coefficient is assigned to each channel response and then averaging is performed through all the channels using the filter coefficients. The filter weights assigned to each channel is chosen to minimize the mean-square error over the early time response, where only the skin reflection exists. The following paragraphs discuss this method in detail (Bond et al., 2003).

To remove the skin artifact from the first channel out of N channel responses, the filter weights could be derived as follows. Suppose that the skin artifact at n^{th} sample of the first channel is to be removed. A window of length $2J+1$ is used to select part of each channel response (except for the first channel) centered at the sample number n. Define $\mathbf{b}_i[n]$, a $(2J+1)\times 1$ vector of these samples from the i^{th} channel as

$$\mathbf{b}_i(n) = [b_i(n-J), \cdots, b_i(n), \cdots, b_i(n+J)]^T,\ 2 \le i \le N \tag{2}$$

Vector $\mathbf{b}_{2N}[n]$ is formed by concatenation of $\mathbf{b}_i$ vectors of channels 2 through N as

$$\mathbf{b}_{2N}(n) = [\mathbf{b}_2^T(n), \cdots, \mathbf{b}_N^T(n)]^T \tag{3}$$

Let $\mathbf{q}_i$ be the filter coefficients in the i^{th} channel; similar to (3), $\mathbf{q}$ is formed as

$$\mathbf{q} = [\mathbf{q}_2^T, \cdots, \mathbf{q}_N^T]^T \tag{4}$$

The error function for this filter is:

$$e = \sum_{n=n_0}^{n_0+m-1} |b_1(n) - \mathbf{q}^T \mathbf{b}_{2N}(n)|^2 \tag{5}$$

In (5) the time interval $n_0 \le n \le (n_0+m-1)$ is part of the signal that contains no backscatter from lesions. The solution to these filter coefficient values are chosen to minimize the error function defined in the (5) which is (Haykin, 1996):

$$\mathbf{q} = \mathbf{R}^{-1}\mathbf{p} \tag{6}$$

where,

$$\mathbf{R} = \frac{1}{m}\sum_{n=n_0}^{n_0+m-1} \mathbf{b}_{2N}(n)\mathbf{b}_{2N}(n)^T \tag{7}$$

and,

$$\mathbf{p} = \frac{1}{m}\sum_{n=n_0}^{n_0+m-1} \mathbf{b}_{2N}(n)b_1(n). \tag{8}$$

High degree of similarity in early time response among the channels, results in an ill-conditioned $\mathbf{R}$ matrix. To prevent error in calculation of $\mathbf{R}^{-1}$ in (6), $\mathbf{R}$ is approximated

by reduced rank $\mathbf{R}_p$ (Bond et al., 2003)

$$\mathbf{R}_p = \sum_{i=1}^{p} \lambda_i \mathbf{u}_i \mathbf{u}_i^T \tag{9}$$

where λ_i is the i^{th} of the first p significant eigenvalues of $\mathbf{R}$ and $\mathbf{u}_i$ is the corresponding eigenvector. $\mathbf{R}_p^{-1}$ is determined by

$$\mathbf{R}_p^{-1} = \sum_{i=1}^{p} \frac{1}{\lambda_i} \mathbf{u}_i \mathbf{u}_i^T. \tag{10}$$

Substituting (10) in (6) yields the filter coefficients. These coefficients could later be used to remove skin response in channel 1 by subtracting the weighted average of $N-1$ other channels as follows

$$b(n)_1 = \sum_n |b_1(n) - \mathbf{q}^T \mathbf{b}_{2N}(n)|^2 \tag{11}$$

The same concept can be used for the other channels.
This algorithm improves the former averaging method in removing the skin response effectively (Zhi & Chin, 2006). Although weighted average can remove the skin artifact more effectively than the simple averaging, it still adds unwanted averaged data from clutter and tumor responses from all signals to each channel response and hence deteriorates the tumor signature (Bond et al., 2003). Another major drawback of this method is the need for a criterion to decide on the moment when the early time response ends. This is because the tumor response should not be included in the MSE minimization used to define filter coefficients otherwise it will be removed from the output. However, the tumor response location is determined in the detection process which is performed after skin removal step and is not a priori knowledge.

4. Frequency domain approach for skin backscatter removal

4.1 Introduction

According to the Geometrical Theory of Diffraction (GTD) (Keller, 1958; Naishadham & Piou, 2004), backscattered signal from a number of scattering points has a pattern in frequency domain. As described in (Cuomo et al., 1999) each scatterer in the view of the antenna will create a harmonic term (pole) in frequency domain response of a UWB pulse radar. This means that the frequency response of the backscattered signal is a combination of some complex harmonic terms with different attenuation coefficient and frequencies. As predicted by GTD, the attenuation coefficient is a function of the shape of the object and its frequency is determined by the distance between the scatterer and the receiver. This representation has interesting applications in UWB microwave radars. Fitting an appropriate model to this pattern helps to reconstruct the signal beyond the bandwidth of the system which leads to a higher image resolution without additional hardware cost. Cumo et. al (Cuomo et al., 1999) have used this bandwidth extrapolation method to estimate the frequency response of the backscattered signal in the gap between two different incoherent subbands.
In this section, we exploit this frequency domain representation to identify and remove the harmonic terms produced by the skin, based on the backscattered energy of the object. After removing the skin related information, the frequency response is reconstructed using the

mathematical model and subsequently the time domain response is reproduced by the inverse Fourier transform. The reconstructed time domain signal is then used to construct an image of the breast medium.

4.2 Model parameters estimation

As stated before, the frequency response of the signal reflected from a number of scattering points could be represented as the sum of a number of complex sinusoids. The number of these terms equals to the number of the scattering points in the view of the antenna and the multiple scattering effect (Moore et al., 1997). Mathematical model of the frequency domain signal is (Piou, 2005),

$$y(f) = \sum_{i=1}^{N} A_i(f) e^{(j\frac{4\pi}{c}R_i)f} \tag{12}$$

where, f is the frequency, c is the speed of light, N is the number of scattering points and R_i is the range of the i^{th} scattering point. $A_i(f)$ is the frequency dependence function corresponding to the i^{th} scattering point. This frequency dependence function is of the form f^{α} and the exponent α is known for some common scattering mechanisms. For example, a flat plate has $\alpha = 1$ or a sphere will have $\alpha = 0$ (Moore et al., 1997). As stated by Cumo et. al (Cuomo et al., 1999), f^{α} scattering behavior can accurately be estimated by exponential functions over a finite bandwidth interval. Hence, the following discrete model can represent the frequency behavior of the reflected signal given in (12) above.

$$y(k) = \sum_{i=1}^{N} a_i e^{-(\alpha_i + j\frac{4\pi}{c}R_i)k\Delta f} \tag{13}$$

where a_i are constant coefficients of the sinusoids, α_i and R_i refer to the frequency decay/growth factor and the range of the i^{th} scatterer, respectively, and Δf is the sampling frequency. In the rest of this section we provide the formulation to estimate model parameters in (13). More details and derivations are available at (Piou, 2005).

4.3 State - space representation of the signal

From the system theory we know that the following state-space equations hold for input-output relation in a linear system.

$$\begin{aligned} \mathbf{x}(k+1) &= \mathbf{A}\mathbf{x}(k) + \mathbf{B}\mathbf{w}(k) \\ \mathbf{y}(k) &= \mathbf{C}\mathbf{x}(k) + \mathbf{w}(k) \end{aligned} \tag{14}$$

where $\mathbf{x}(k)$ is the state vector, $\mathbf{w}(k)$ is the input vector and $\mathbf{y}(k)$ is the output of the system. $\mathbf{A}$, $\mathbf{B}$ and $\mathbf{C}$ are matrices characterizing the system and define its state-space behavior. The transfer function of the system described in (14) is given in (15).

$$\mathbf{T}(z) = \frac{\mathbf{Y}(z)}{\mathbf{X}(z)} = \mathbf{C}(z\mathbf{I} - \mathbf{A})^{-1}\mathbf{B} + 1 \tag{15}$$

The impulse response of such system in general comprises a number of complex sinusoids or poles of the system which are the roots of the denominator or as seen in (15) are the

eigenvalues of **A**, the open-loop matrix of the system. Hence, the output signal of the system $y(k)$ can be written as

$$y(k) = \sum_{i=1}^{M} a_i e^{-(\alpha_i + j\beta_i)k\Delta t} \tag{16}$$

In (16) M is the number of the poles of the system or the eigenvalues of **A**, a_i are the constant coefficients of each complex sinusoid and α_i and β_i are the damping factor and frequency of the i^{th} harmonic, respectively. Δt is the sampling time interval.
Comparing (16) and (13) reveals that the frequency response of the backscattered signal and the impulse response of a linear system have a similar mathematical structure. Thus, we can use the mathematics of linear system identification to estimate the parameters of the frequency model for the backscattered data. In the rest of this section the formulation to obtain model parameters is presented.
Suppose that the frequency response of the backscattered signal is the impulse response of a hypothetical linear system. Here we try to extract the system matrices and consequently a model for the impulse response based on the eigenvalues or poles of this hypothetical system. As mentioned before, we can derive the desired frequency model parameters from this impulse response model.
The process of finding the hypothetical system matrices involves forming forward prediction or Hankel matrix from the sample data of the frequency response of the backscattered signal and deriving **A** through singular value decomposition of **H**, the Hankel matrix which is defined as follows,

$$\mathbf{H} = \begin{pmatrix} y(1) & \cdots & y(L) \\ \vdots & \ddots & \vdots \\ y(N-L+1) & \cdots & y(N) \end{pmatrix} \tag{17}$$

where, $y(i)$ are the samples of frequency domain response of the backscattered data, N is the number of data samples and L is chosen as $N/3$ (Naishadham & Piou, 2004). By singular value decomposition, **H** is decomposed into three matrices,

$$\mathbf{H} = \mathbf{U}\boldsymbol{\Sigma}\mathbf{V}^* \tag{18}$$

In which **U** is the left unitary matrix, $\mathbf{V}^*$ is the right unitary matrix, and $\boldsymbol{\Sigma}$ is a diagonal matrix containing singular values of **H** in a descending order. $(*)$ denotes the complex conjugate and transpose.
Singular values of **H** could be separated into two subspaces, the signal plus noise subspace and the only noise subspace. If the SNR value is high enough there would be a sharp transition between singular values of the signal and those of noise. The criterion for separating the two parts is described in (Naishadham & Piou, 2005). Hence, **U**, $\boldsymbol{\Sigma}$, $\mathbf{V}^*$ could be divided into two different subspaces as follows,

$$\mathbf{H} = \begin{bmatrix} \mathbf{U_{sn}} & \mathbf{U_n} \end{bmatrix} \begin{bmatrix} \boldsymbol{\Sigma}_{\mathbf{sn}} & 0 \\ 0 & \boldsymbol{\Sigma}_{\mathbf{n}} \end{bmatrix} \begin{bmatrix} \mathbf{V}^*_{\mathbf{sn}} \\ \mathbf{V}^*_{\mathbf{n}} \end{bmatrix} \tag{19}$$

which in (19) the subscripts 'sn' and 'n' refer to the signal-noise and noise subspaces respectively. Removing the noise part, $\tilde{\mathbf{H}}$ can be formed as follows,

$$\tilde{\mathbf{H}} = \mathbf{U_{sn}}\boldsymbol{\Sigma}_{\mathbf{sn}}\mathbf{V}^*_{\mathbf{sn}} \tag{20}$$

Using the balanced coordinate method (Piou, 2005), $\tilde{\mathbf{H}}$ could further be factorized as

$$\tilde{\mathbf{H}} = \mathbf{\Omega\Gamma} \tag{21}$$

where

$$\mathbf{\Omega} = \mathbf{U_{sn}}\mathbf{\Sigma_{sn}}^{1/2} \text{ and } \mathbf{\Gamma} = \mathbf{\Sigma_{sn}}^{1/2}\mathbf{V_{sn}^*} \tag{22}$$

where $\mathbf{\Omega}$ and $\mathbf{\Gamma}$ are the observability and controllability matrices respectively. $\mathbf{A}$ could be derived from both the observability or the controllability matrices, here $\mathbf{\Omega}$ is used to derive $\mathbf{A}$.

$$\mathbf{A} = (\mathbf{\Omega_{-rl}^*\Omega_{-rl}})^{-1}(\mathbf{\Omega_{-rl}\Omega_{-rf}}) \tag{23}$$

where $\mathbf{\Omega_{-rl}}$ and $\mathbf{\Omega_{-rf}}$ are obtained by removing the last and first rows of $\mathbf{\Omega}$, respectively. Now α_i and R_i are related to the eigenvalues of $\mathbf{A}$ by:

$$\alpha_i = \frac{-log|\lambda_i|}{\Delta f} \text{ and } R_i = -c\frac{\Phi_i}{4\pi\Delta f} \tag{24}$$

where R_i is the range and α_i is the damping factor of the sinusoid related to the i^{th} scattering point. Φ_i is the phase of λ_i, the i^{th} eigenvalue of $\mathbf{A}$. To find the constant coefficients a_i we use the following equation,

$$a_i = \frac{(\mathbf{Cm_i})(\mathbf{v_iB})}{\lambda_i^{f_1/\Delta f}} \tag{25}$$

where $\mathbf{m_i}$ are eigenvectors of $\mathbf{A}$, and $\mathbf{v_i}$ are defined as

$$\mathbf{V} = [\mathbf{m_1} \cdots \mathbf{m_p}]^{-1} = \begin{bmatrix} \mathbf{v_1} \\ \vdots \\ \mathbf{v_p} \end{bmatrix} \tag{26}$$

In (25), $\mathbf{C}$ is the first row of $\mathbf{\Omega}$, f_1 is the carrier frequency of the pulse and the k^{th} element of frequency vector is related to carrier frequency by

$$f_k = f_1 + (k-1)\Delta f \tag{27}$$

To derive $\mathbf{B}$, $\mathbf{\Omega_N}$ is defined,

$$\mathbf{\Omega_N} = \begin{bmatrix} \mathbf{C} \\ \mathbf{CA} \\ \vdots \\ \mathbf{CA}^{N-1} \end{bmatrix} \tag{28}$$

and $\mathbf{B}$ is obtained by,

$$\mathbf{B} = (\mathbf{\Omega_N^*\Omega_N})^{-1}(\mathbf{\Omega_N^*y^T}) \tag{29}$$

where $\mathbf{y}$ is the vector of the frequency samples of the backscattered data. Now a_i could be derived from (25). Now that all the parameters of the model in (13) are derived the frequency response of the system could be reconstructed.

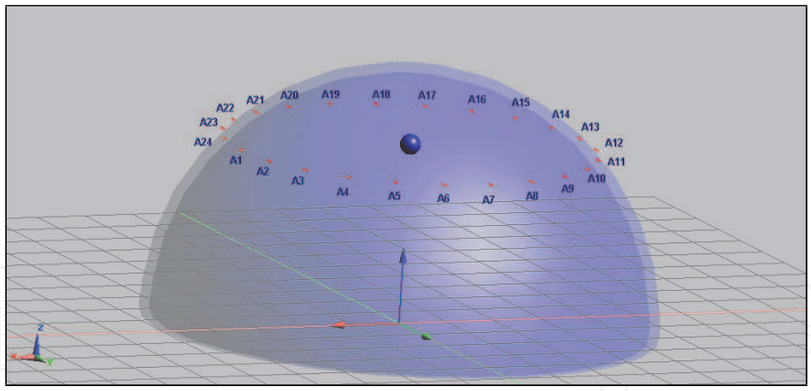

Fig. 3. Antenna array and tumor configuration

5. Evaluation of the performance of the frequency domain skin removal in comparison with other methods

The present section applies the frequency domain skin removal method described in section 4 in different scenarios and compares its performance with other methods. The focus in the first part is more on details of applying the formulation provided in Section 4 on a simplified breast model. The second part will apply the method in a more realistic scenario and compares the results with the other methods.

5.1 Simplified Breast Model

As discussed in Section 4, the backscattered signal of a UWB pulse is the summation of some harmonic terms. The number of these terms depend on the number of scattering points and the multiple scattering effect. Each harmonic term consists of a complex exponential and a coefficient. The argument of this complex exponential is the pole of the hypothetical system mentioned in Section 4. By removing the poles corresponding to the skin reflection from the frequency domain signal, all the skin related information will be removed from time domain. The process is as follows.

The received signals are first converted into frequency domain using Fast Fourier Transform (FFT) algorithm. The frequency domain signals are then processed to extract the model parameters stated in the previous section. Among these parameters, a_is are directly related to the amplitudes of each of the backscattered pulses. This can be explained as follows. In Equation (13), a_i is a complex coefficient which can be written as $|a_i|e^{j\theta_i}$ where θ_i is the phase of a_i. Taking the inverse Fourier transform of Equation (13) yields

$$x(t) = \sum_{i=1}^{N} |a_i| \frac{2\alpha_i cos(\theta_i)}{\alpha_i^2 + (t - 4\pi R_i/c)^2} \tag{30}$$

As seen in Equation (30), $|a_i|$ is proportional to the amplitude of the pulse in the time domain. However, the amplitude of the pulse backscattered from the tumor is much smaller than the skin backscatter. Hence, a threshold could be defined to remove poles with dominant a_i values from the frequency response of the signal. Removing the poles over the stated threshold ensures that only the poles corresponding to the skin will be removed from the signal. This will remove the skin effect both in the early time and the late time responses as the elimination in frequency domain will affect the whole time domain signal. Hence, the tumor reflection will

be preserved without the skin late time response interference in the signal. After removing the skin related poles, the frequency domain signal is reconstructed using the mathematical model (13) and then converted back into the time domain using the inverse-FFT algorithm. Hence, the reconstructed signal will only contain contributions from the tumor and clutter. Clutter will be rejected later using confocal imaging algorithm described in Section 1. We will

Ant. No.	x	y	z	Ant. No.	x	y	z
1	35.71	0	35	13	-35.71	0	35
2	34.50	10.24	35	14	-34.50	-10.24	35
3	30.93	17.86	35	15	-30.93	-17.86	35
4	25.26	26.26	35	16	-25.26	-26.26	35
5	17.86	30.93	35	17	-17.86	-30.93	35
6	9.24	35.50	35	18	-9.24	-35.50	35
7	0	35.71	35	19	0	-35.71	35
8	-9.24	35.50	35	20	9.24	-35.50	35
9	-17.86	30.93	35	21	17.86	-30.93	35
10	-25.50	26.26	35	22	25.26	-26.26	35
11	-30.93	17.86	35	23	30.93	-17.86	35
12	-34.50	10.24	35	24	34.50	-10.24	35

Table 1. Antenna Arrangement

first describe the idea in detail using a simplified simulated breast model using SEMCAD X (version 13) software package for an antenna array with 24 elements in a circular configuration around the breast in order to show the ability of the method to remove the skin reflection from the backscattered signal. The breast medium is modeled by a hemisphere with a radius of 50mm and thickness of 2mm as the skin layer. A spherical tumor with a radius of 2mm is placed on the central axis of the hemisphere and at a height of 35mm from the center of the hemisphere (x = 0mm, y = 0mm, z = 35mm). The model and the antenna locations are shown in Figure 3 and Table 1 respectively. The relative permittivities of the skin and breast tissues are set to the values given by (Fear et al., 2002) ($\epsilon_r(skin) = 36$, $\epsilon_r(tissue) = 9$). The dielectric value assigned to the tumor is the measured dielectric value of the malignant tumor $\epsilon_r = 50$ (Fear et al., 2002). Figure 4 shows the signal received in channel 1 and its spectrum. As the

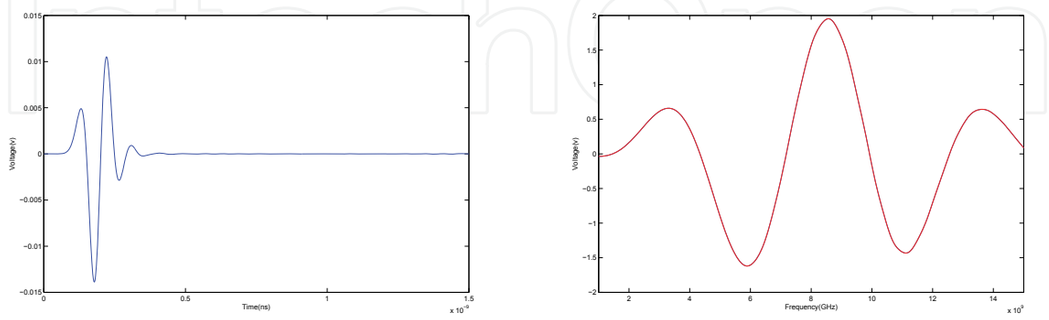

(a) Signal received in channel 1

(b) Frequency response of the signal received in channel 1

Fig. 4. Signal received in channel 1 and its frequency response

skin reflects the largest energy among the reflectors in the breast medium, the high energy dominant poles in the frequency domain will correspond to the skin backscatter. Hence a threshold may be used to remove these dominant poles. The threshold is defined based on the ratio of the backscattered energies of the skin to the tumor and is obtained as follows. We fix the threshold value a little higher than the ratio of the largest possible peak tumor to the skin response times the maximum reflection coefficient value a_i. The maximum reflection coefficient corresponds to the largest scatterer which is the skin surface. Hence, by removing all the poles with a_i values larger than this threshold from early time response we make sure that only reflections larger than the tumor reflection is removed from the signal. Many factors can affect the skin to tumor response ratio and more study is needed to consider all the factors affecting this ratio and obtain an optimized threshold value. Here, to show the basic idea of the current method, we consider three factors, tumor size, skin thickness and tumor location to determine the highest possible ratio. To experimentally estimate the highest possible skin to tumor response ratio, the tumor reflection is isolated from the other reflections by performing two different simulations. One simulation is done without the tumor and the second one is with the tumor. Subtracting the results of these simulations yields the tumor signature. According to (Ulger et al., 2003) breast skin thickness varies in the range of 0.5-3.1mm; hence two extreme cases (0.5 and 3.1mm) are simulated in the experiments. The tumor size is set 2mm and 5mm which is well within the range of the early breast cancer. Then the tumor location is varied on the line connecting the center to the antenna location from the center of the breast hemisphere to 5mm below the inner layer of the skin as the tumors so close to the skin can be detected by examining the surface of the breast.
Tables 2 and 3 show the tumor to skin peak response ratio for the skin thickness of 0.5mm and 3.1mm respectively.

Location \ Tumor size	2mm	5mm
Center	9.04E-05	1.81E-04
Under The Skin	3.80E-03	5.20E-03

Table 2. Skin to Tumor Ratio (Skin Thickness: 0.5mm)

Location \ Tumor size	2mm	5mm
Center	7.72E-05	1.69E-04
Under The Skin	2.10E-03	4.00E-03

Table 3. Skin to Tumor Ratio (Skin Thickness: 3.1mm)

As expected, the tumor to skin response ratio increases as the tumor size increases. As seen in the tables, the maximum ratio is obtained when the tumor radius is 5mm and is located 5mm below the skin, the highest tumor to skin response ratio is 0.0021, i.e. the skin reflection is about 476 times stronger than the largest tumor reflection. Hence, by setting the threshold a little larger than 0.21% of the largest reflection coefficient (a_{max}) and removing all the poles with a_i values larger than this threshold from early time response we ensure that all the reflections larger than the tumor reflection is removed from the signal. This would be true in all other cases as we chose the largest possible tumor response to define the threshold.
Here, we chose 0.0025 $\times$ the largest reflection coefficient as the threshold value. The poles extracted from the signal in channel 1 are shown in Table 4; Eliminated poles are indicated by a '*'.

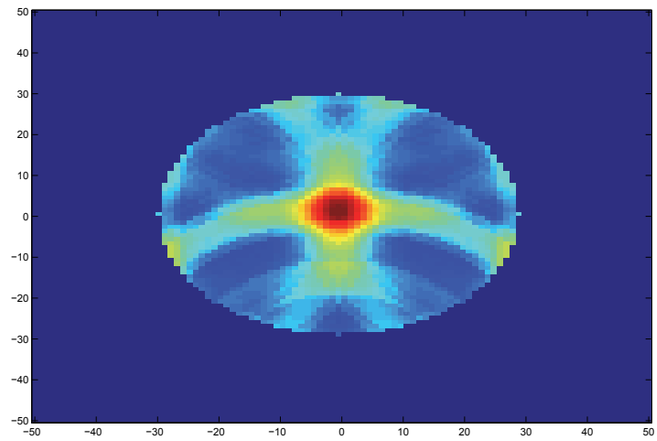

Fig. 5. Confocal imaging of the breast after removing the skin reflection

Figure 6 shows the backscattered signal after removing the skin reflection. In the figure, solid line represents the reconstructed signal super-imposed with the original signal represented by the dotted line. As seen in the figure the skin backscatter is removed from the signal. Figure 7

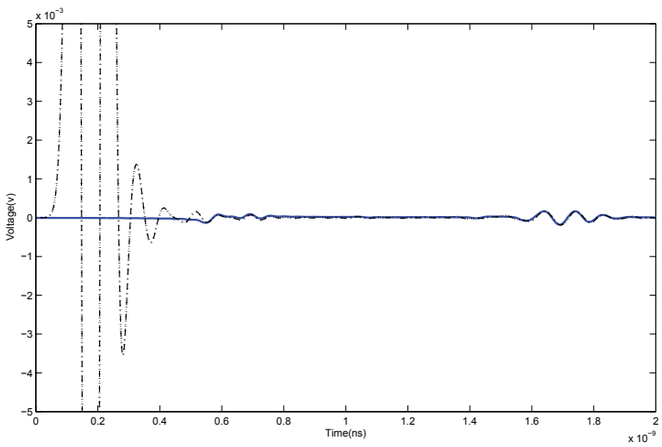

Fig. 6. The dotted line shows the original signal and the solid line is the signal after skin backscatter removal.

shows a larger view of the late time part of the response. As shown in the figure, the late time part of the signal, where the tumor response exists, has not been affected significantly.

5.2 Comparison with the Averaging and Weighted Average Methods

In this section, the performance of the frequency domain method is compared with the averaging (Li & Hagness, 2001) and weighted average filter (Bond et al., 2003). To make the breast model more realistic, the mapping of the dielectric values inside the breast medium is obtained from an MRI image of a real breast as shown in Figure 8. The clutter produced due to the heterogeneity of the breast tissue has significant effect on the effectiveness of the skin subtraction methods. In the averaging based methods, the averaged clutter from all other

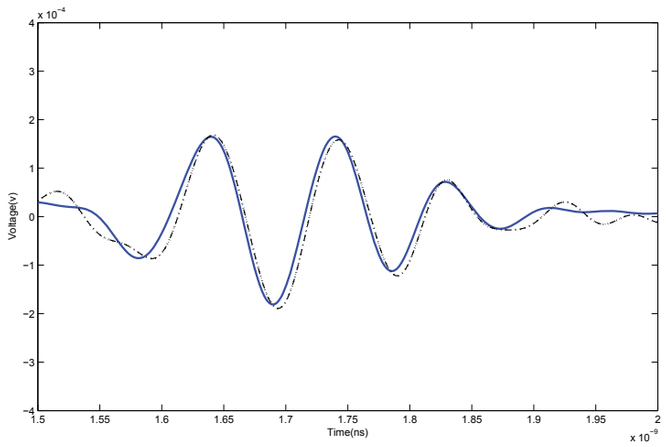

Fig. 7. The late time response of the reconstructed signal (line with dots) vs. the original signal (solid)

Pole No.	Reflection Coefficient	Pole No.	Reflection Coefficient
1	0.006030024	16	0.000576253
2	*0.330168871	17	0.000817322
3	*2.769236715	18	0.001800899
4	*8.978906551	19	0.003023339
5	*17.21322261 (MAX)	20	0.002570893
6	*16.81465757	21	0.000965909
7	*7.610199166	22	0.00044818
8	*1.504612836	23	0.000653675
9	*0.255119890	24	0.001118491
10	*0.052006092	25	0.000111348
11	0.005144400	26	0.00232989
12	0.005526546	27	0.000489255
13	0.004168027	28	0.010678232
14	0.001581127	29	0.022283477
15	0.001108609	30	0.022266937

Table 4. Reflection Coefficients(Eliminated poles are identified by *)

channels is added to each channel and makes the tumor detection even more difficult. As seen in Figure 8, different dielectric constants of the breast internal regions appear as varying intensities in the gray scale image. The scale for this mapping is given beneath the image. Here, the regions with different dielectric values are approximated by spheres. The radius of the sphere is chosen as the circumference of the region divided by 2π. The center of the spheres are located at the same height and distance as the center of the corresponding region from the center of the breast. Assume that the vertical axis in Figure 8 is z and the horizontal axis is x in the Cartesian coordinates. In this configuration, y would have an inward direction perpendicular to the xz plane. To make the model 3D, the angle ϕ_i (between the position vectors of i^{th} sphere center and x axis) are chosen randomly in the interval $[-\pi, \pi]$. In this experiment, the tumor coordinates are x=0, y=0, z=35 (mm). Figure 9 shows the model obtained. The locations of the sphere centers are given in Table 5.

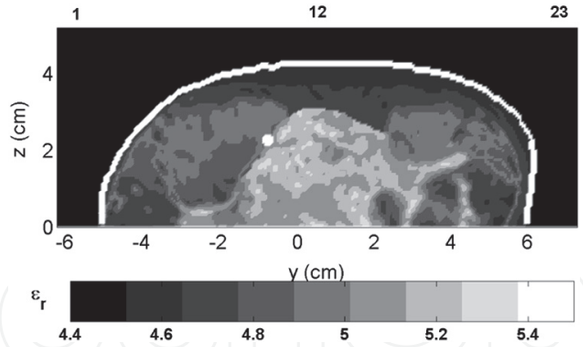

Fig. 8. 2D mapping of the dielectric values of the different regions of the breast tissue(source:(Kosmas & Rappaport, 2005))

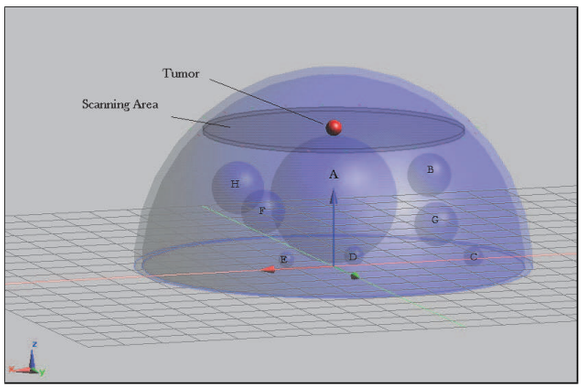

Fig. 9. 3D Model Constructed based on MRI image, shaded region shows the scanning area

Region	x	y	z	ϵ_r	Region	x	y	z	ϵ_r
A	0	0	17	5.3	E	16	10	4	4.8
B	-25	0.9	22	5.2	F	11	-9	11	5
C	-28	26	5	4.8	G	-36	-25	5.5	5
D	4	27	7	4.8	H	27	4.7	22	5.2

Table 5. Dielectric region centers (mm)

In this model, the skin layer thickness is set as 2mm. The antenna placement, physical parameters of the normal breast tissue and tumor are set as described in the previous section. As for the clutter regions, dielectric values are obtained from the MRI image as stated above. These values are given in Table 5.

The skin reflection is removed from the simulated backscattered signals using all three methods: frequency domain approach, averaging and weighted average filter to compare the performance of these methods. A 2D image of the breast is formed by applying confocal imaging process on the processed signals. The resulting images from the three methods are shown in Figure 10. Due to the symmetry of the tumor location to the antenna elements in the array, the tumor response is totally eliminated from the image processed by averaging and filtering methods. This is because, the tumor response will add coherently in the averaging process (due to the symmetry) and hence will appear in the average signal. Hence, subtracting the average removes the tumor backscatter as well as the skin backscatter. However, in frequency domain approach, each signal is processed separately and no other data is added

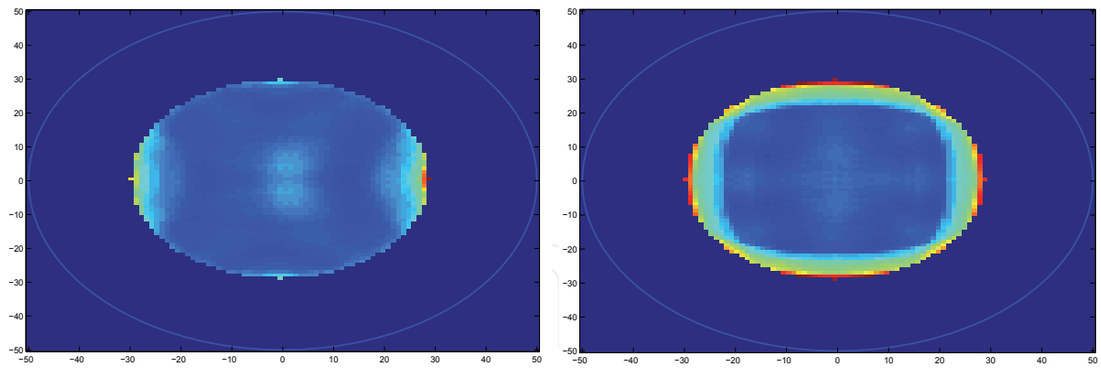

(a) Averaging (b) Weighted Average Filter

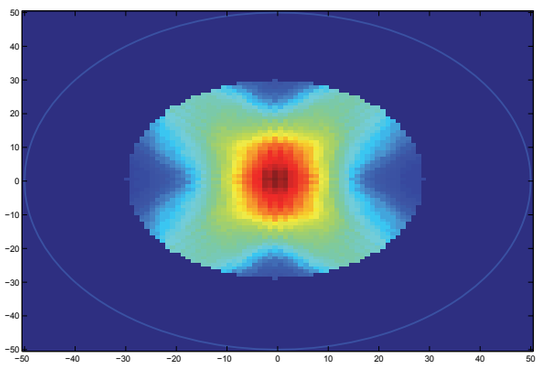

(c) Pole Removal

Fig. 10. Breast images using three skin subtraction methods: Averaging(a), Weighted Average(b), Pole removal(c)

to or subtracted from the signal, the tumor signature remains intact. This is confirmed in Figure 10. As seen in the figure, the tumor is detected at the central axis of the breast.
To compare the performance of the three methods in general case, the tumor is located in off center coordinates (x = 35 , y = 0, z = 15). The other parameters of the model are the same as the previous model.
Again, the skin reflection is removed using the three mentioned methods. The results are shown in Figure 11.
As the figure reveals, all three methods have eliminated the skin effect and the tumor is detected in the resulting image. To further evaluate the performance of the skin removal methods, the peak Tumor to Clutter Ratio (TCR) for the three methods is compared in Table 6. As seen in the table, the tumor to clutter ratio is the highest for frequency domain approach

Skin-Removal Method	TCR
Pole-Removal	3.831
Weighted Average	2.082
Averaging	1.837

Table 6. Tumor to Clutter Ratio (TCR)

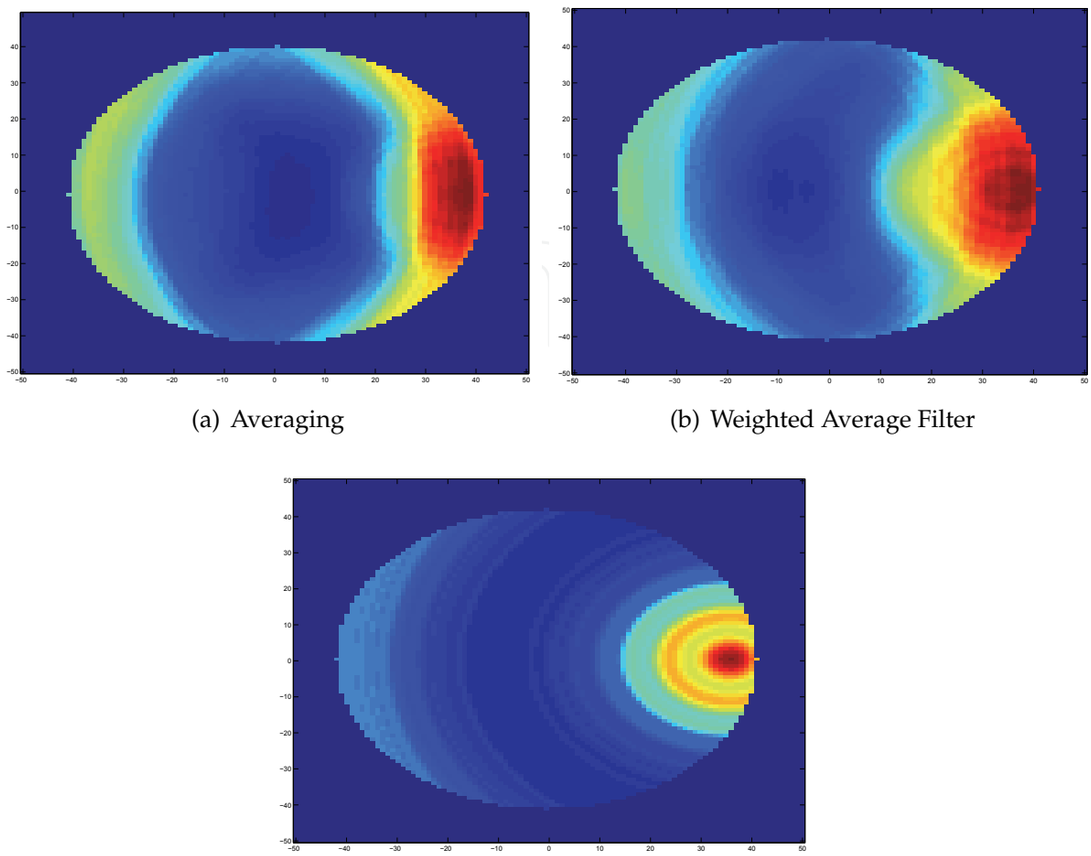

(a) Averaging (b) Weighted Average Filter

(c) Pole Removal

Fig. 11. Tumor at: x = 35, y = 0, z = 15 (mm), Averaging(a), Weighted Average(b), Pole removal(c)

and is the lowest for simple averaging. This is expected since pole removal method processes each signal individually unlike the other two methods which add clutter from other signals and degrade the tumor reflection.

6. Conclusion

The high contrast in the dielectric value of the skin relative to the normal breast tissue and air produces a strong backscatter in UWB breast cancer detection method. Such strong backscatter can totally mask the tumor reflection and hence has to be removed from the signal. Currently, two methods are used in practice to remove skin reflection. Both methods exploit the similarity of the skin reflection in the signals collected by an array of antennas to reconstruct and remove the skin reflection. Although these methods can significantly reduce the skin contribution in the backscattered signal, they have some shortcomings. Both methods use averaging to estimate the skin backscatter from the signals collected in different elements of the antenna array. As a result, if the tumor is approximately equidistant to some of the elements of the array, its reflection will suffer a high attenuation in the processed signals. This will make the tumor detection very difficult or even impossible. Another problem of the

averaging based methods is that they add the averaged version of the noise and clutter from all channels to each individual channel which makes the tumor detection even more difficult. In addition, as the tumor reflection should not be included in the skin reflection estimation process, these methods need to determine the early time part of the signal where only the skin reflection exists. However, the location of the tumor in the signal is not known prior to the detection process.

This work introduces a new approach in removing the skin reflection from the backscattered signal in UWB breast cancer detection. In this approach, the backscattered signals are analyzed in frequency domain to identify and remove the skin related information from the frequency response. Based on Geometrical Theory of Diffraction (GTD), a mathematical model is applied on the frequency response of the signal. Then, the terms corresponding to the skin are removed from the model and the signal is reconstructed. Performance of this method is compared with the other existing methods in Section 5. As shown in Section 5, the frequency domain approach can detect the tumor even when it is equidistant to all the elements of the array. Besides, no extra noise and clutter is added to the signal as each signal is processed individually. Thus, the frequency domain approach shows higher tumor to clutter ratio in comparison with the other two methods. However, more investigations is needed to determine some parameters of the process such as the threshold used to remove the skin related terms from the frequency response. To optimize parameters such as the number of the antenna elements needed in the array, type of the antenna, pulse shape, etc. the method has to be applied on more realistic scenarios similar to the human breast.

7. References

Bond, E., Li, X., Hagness, S. & Van Veen, B. (2003). Microwave imaging via space-time beamforming for early detection of breast cancer, *IEEE Transactions On Antennas and Propagation* 51(8): 1690–1705.

Cuomo, K., Piou, J. & Mayhan, J. (1999). Ultrawide-band coherent processing, *IEEE Microwave Magazine* 47(6): 1094–1107.

Fear, E., Li, X., Hagness, S. & Stuchly, M. (2002). Confocal microwave imaging for breast cancer detection: Localization of tumors in three dimensions, *IEEE Transactions on Biomedical Engineering* 49: 812–821.

Fear, E. & Stuchly, M. (2000). Microwave detection of breast cancer, *IEEE Transactions On Microwave Theory And Techniques* 48(11): 1854 – 1863.

Hagness, S., Taflove, A. & Bridges, J. (1998). Two dimensional FDTD analysis of a pulsed microwave confocal system for breast cancer detection: Fixed-focus and antenna-array sensors, *IEEE Trans. Biomed. Eng.* 45: 1470–1479.

Haykin, S. (1996). *Adaptive Filter Theory*, 3rd edn, Prentice-Hall.

J. Elwood and B. Cox and A. Richardson (1993). The effectiveness of breast cancer screening by mammography in younger women, *The Online journal of current clinical trials* 32. URL: *http://www.ncbi.nlm.nih.gov/pubmed/8305999*

Keller, J. (1958). *A geometrical theory of diffraction*, Courant Institute of Mathematical Sciences, New York University.

Kosmas, P. & Rappaport, C. (2005). Time reversal with the FDTD method for microwave breast cancer detection, *IEEE Transactions on microwave theory and techniques* 53(7): 2317–2322.

Li, X. & Hagness, S. (2001). A confocal microwave imaging algorithm for breast cancer detection, *IEEE Microwave and Wireless Components Letters* 11(3): 130–132.

Moore, T., Zuerndorfer, B. & Burt, E. (1997). Enhanced imagery using spectral-estimation-based techniques, *Lincoln Laboratory Journal* 10(2): 171–186.

Naishadham, K. & Piou, J. (2004). A super-resolution method for extraction of modal responses in wideband data, *IEEE Antennas and Propagation Society International Symposium* 4: 4168–4171.

Naishadham, K. & Piou, J. (2005). State-space spectral estimation of characteristic electromagnetic responses in wideband data, *IEEE Antennas and Wireless Propagation Letters* 4: 406–409.

Piou, J. (2005). A state identification method for 1-d measurements with gaps, *Proc. American Institute of Aeronautics and Astronautics Guidance Navigation and Control Conf.* .

American Cancer Society (ACS) (2007). What are the key statistics for breast cancer? URL: *http://www.cancer.org/docroot/CRI/content/CRI_2_4_1X_What_are_the_key_statistics_for_breast_cancer_5.asp*

Center for Disease Control and Prevention (CDC) (2007). Statistics. URL: *http://www.cdc.gov/cancer/breast/statistics/*

Ulger, H., Erdogan, N., Kumanlioglu, S. & Unur, E. (2003). Effect of age, breast size, menopausal and hormonal status on mammographic skin thickness, *Skin Research and Technology* 9: 284–289.

Zhi, W. & Chin, F. (2006). Entropy-based time window for artifact removal in uwb imaging of breast cancer detection, *IEEE Signal Processing Letters* 13(10): 585–588.

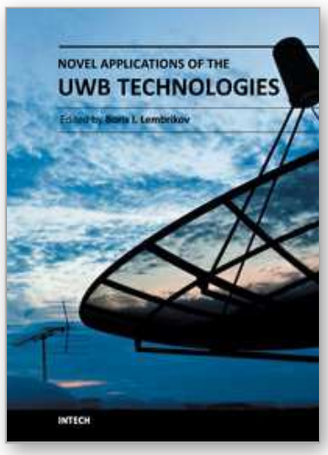

Novel Applications of the UWB Technologies

Edited by Dr. Boris Lembrikov

ISBN 978-953-307-324-8
Hard cover, 440 pages
Publisher InTech
Published online 01, August, 2011
Published in print edition August, 2011

Ultra wideband (UWB) communication systems are characterized by high data rates, low cost, multipath immunity, and low power transmission. In 2002, the Federal Communication Commission (FCC) legalized low power UWB emission between 3.1 GHz and 10.6 GHz for indoor communication devices stimulating rapid development of UWB technologies and applications. The proposed book Novel Applications of the UWB Technologies consists of 5 parts and 20 chapters concerning the general problems of UWB communication systems, and novel UWB applications in personal area networks (PANs), medicine, radars and localization systems. The book will be interesting for engineers and researchers occupied in the field of UWB technology.

InTech Europe
University Campus STeP Ri
Slavka Krautzeka 83/A
51000 Rijeka, Croatia
Phone: +385 (51) 770 447
Fax: +385 (51) 686 166
www.intechopen.com

InTech China
Unit 405, Office Block, Hotel Equatorial Shanghai
No.65, Yan An Road (West), Shanghai, 200040, China
中国上海市延安西路65号上海国际贵都大饭店办公楼405单元
Phone: +86-21-62489820
Fax: +86-21-62489821

IntechOpen